Semiconductor Physics, Quantum Electronics & Optoelectronics, 2015. V. 18, N 1. P. 1-11.
doi: 10.15407/ spqeo18.01.001

PACS 72.20.Ht, 72.20.Dp, 73.23.-b, 85.35.-p

Theory of high-field electron transport in the heterostructures $Al_xGa_{1-x}As/GaAs/Al_xGa_{1-x}As$ with delta-doped barriers. Effect of real-space transfer

V.V. Korotyeyev
V. Lashkaryov Institute of Semiconductor Physics, Department of Theoretical Physics, 41, prospect Nauky, 03028 Kyiv, Ukraine; e-mail: koroteev@ukr.net

Abstract. Steady-state electric characteristics of quantum heterostructures $Al_xGa_{1-x}As/GaAs/Al_xGa_{1-x}As$ with δ -doped barriers have been analyzed in this work. It has been shown that at high doping the additional low-conductive channels are formed in the barrier layers. Current-voltage characteristics of the structure were obtained in the wide interval of applied electric fields up to several kV/cm being based on the solution of Boltzmann transport equation. It has been found that in the electric fields higher than 1 kV/cm the effect of exchange of the carriers between the high-conductive channel of the GaAs quantum well and the channels in the AlGaAs barriers becomes essential. This effect gives rise to the appearance of the strongly nonlinear current-voltage characteristics with a portion of negative differential conductivity. The developed model of heterostructure is adequate to those recently fabricated and studied by Prof. Sarbey's group. The obtained results explain some observation of this paper. It has been found that the effect of electron real-space transfer takes place at both low temperatures and room temperatures, which opens perspectives to design novel type nanostructured current controlled devices.

Keywords: quantum heterostructures, real-space transfer, electron transport.

Manuscript received 30.10.14; revised version received 17.11.14; accepted for publication 19.02.15; published online 26.02.15.

1. Introduction

In recent decades, modulation-doped quantum well heterostructures received great attention due to their unique electronic properties allowing numerous applications in science, medicine and industry. One of the important areas for these applications is the high-frequency and high-power electronics [1-4], which relates to fabrication of solid-state modulators and generators of electromagnetic radiation in the sub-THz and THz spectral ranges [5, 6]. Quantum wells made of different semiconductor materials such as GaN/AlGaN [7-9], GaAs/AlGaAs [10], InGaAs/InAlAs [11] show good perspectives to realize these goals. For generation of high-frequency radiation, several mechanisms of the current instabilities are used, all of them are based on the action of strong applied electric fields [12-16].

Among them, it should be noted the effect of the electron real-space transfer (RST) that was observed in the quantum heterostructures. Usually, this effect is detected in measurements of current-voltage (*I-V*) characteristics as an interval with negative differential conductivity [17, 18]. The phenomena of RST is referred to as transfer of hot electrons in the direction perpendicular to heterolayers due to the heating effect in the electric fields applied in the direction along hetero-layers. There are number of papers published in the past where RST was measured and explained [19-22].

Recently, the effect of RST was observed in the novel, high-quality *n*-AlGaAs/GaAs/AlGaAs hetero-structures with δ-like doped layers in the AlGaAs barriers [23]. The values of impurity concentrations and position of δ-layer seem to be quite enough to form the low-mobility side well (SW) and ensure the effective exchange of carriers between SW and structural high-mobility GaAs quantum well (QW). At electron heating, SW will be effectively filled up by electrons from high-mobility QW, as a result, the total conductivity of structure is decreased that can lead to the non-linear current-voltage characteristics with well-pronounced saturation or even dropping behavior. Apparently, this redistribution of electrons can also change the high-frequency conductivity and transparency of heterostructure for electromagnetic radiation, as well. This idea can be used in development of very fast, electrically-tuned modulator of high-frequency radiation [24].

The aim of this paper is to offer the analytical theory of the RST phenomenon in the heterostructures with δ-doped barriers. To properly describe the high-field electron transport under condition of the real-space transfer, it is necessary to account the electron scattering mechanisms at high kinetic energies and modification of electrostatic potential at charge redistribution induced by the applied strong lateral field. In particularly, the calculation model of electrostatic characteristics of heterostructure is formulated in Section 2. The model of the high-field electron transport in the high-mobility QW, and the model of electron redistribution between QW and SW are discussed in Section 3. The results of self-consistent calculations of potential profiles of the structure, distributions of electrons at different applied electric fields, field dependences of the drift velocity and electron temperature, and the current-voltage characteristics are presented in Section 4. Finally, the main results are summarized in Section 5.

2. Electrostatics of quantum well heterostructure with δ-doped barriers

Discussion of the electrostatic model for the heterostructure under consideration is separated by two interrelated parts. The first one relates to the description of well GaAs layer, and the second one does to description of barrier $Al_xGa_{1-x}As$ layers.

2.1. Electrostatics of the well layer

Let us consider the symmetric heterostructure $Al_xGa_{1-x}As/GaAs/Al_xGa_{1-x}As$ with layers grown along *z*-axis. The structural GaAs quantum well has the width *d*. The reference point for the *z*-variable corresponds to the middle of QW. The electrostatic profile, $\phi(z)$, and wave functions of electron, $\psi(z)$, inside QW can be obtained by means of the self-consistent solution of Schroedinger and Poisson equations as follows:

$$\begin{cases} -\dfrac{\hbar^2}{2m^*}\dfrac{d^2\psi(z)}{dz^2} + \left[V(z) - e\phi(z) - E_1\right]\psi(z) = 0, \\ \dfrac{d^2\phi(z)}{dz^2} = \dfrac{4\pi e}{\kappa_0} n_e^{2D} \left|\psi(z)\right|^2, \end{cases} \tag{1}$$

where $V(z)$ is the heterostructural built-in potential energy, $V(z) = -V_b$ at $|z| < d/2$ and $V(z) = 0$ at $|z| > d/2$ (V_b is the conduction band offset GaAs and $Al_xGa_{1-x}As$ materials and one depends on chemical composition, *x*), $\phi(z)$ is the electrostatic potential induced by the finite values of the electron concentration, n_e^{2D}, inside QW. Generally speaking, the several discrete energy levels of size quantization corresponding to different minima of the conduction band can exist in QW as a subject to *x* and *d*. In the model reported here, we restrict ourselves by the consideration of these parameters for the heterostructure (see Section 3) at which only the lowest level of size quantization, E_1, corresponding to the Γ-valley of GaAs is found in QW and populated by electrons with the effective mass, m^*. This medium has the dielectric constant κ_0. The difference between dielectric constants of the well and barrier materials will be neglected. It is convenient to rewrite the system (1) in the following compact dimensionless form:

$$\begin{cases} \psi'' + a_V\left[\Phi + E_1\right]\psi = 0, \\ \Phi'' - \lambda_e^{2D}\left|\psi(z)\right|^2 = 0, \end{cases} \tag{2}$$

where accents denote the spatial derivative with respect to the dimensionless variable $\zeta = z/d$. The introduced dimensionless parameters are as follows: $a_V = 2m^* k_B T d^2/\hbar^2$, $\lambda_e^{2D} = 4\pi e^2 n_e^{2D} d/\kappa_0 k_B T$, $\Phi = \left(e\phi(z) - V(z)\right)/k_B T$ and $E_1 = E_1/k_B T$, where T is the equilibrium lattice temperature.

The solution of the system of nonlinear differential equations (2) can be found numerically, using the following boundary condition:

$$\begin{aligned} &\psi(1/2) = 0 \quad (a); \quad \psi'(0) = 0 \quad (b); \\ &\Phi(1/2) = v_b \quad (c); \; \Phi'(0) = 0 \quad (d) \end{aligned} \tag{3}$$

with $v_b = V_b/k_B T$. The condition (*a*) assumes that electrons are strongly localized inside QW (approximation of deep QWs), conditions (*b*) and (*d*) are the results of the symmetry properties of the wave function in the ground state and spatial symmetry of the heterostructure relatively to the point $z = 0$, respectively. The condition (*c*) is due to the choice of the reference system. Finally, the unknown parameter E_1 is looked for from the normalization condition of the wave function:

$$\int_{-1}^{1} d\zeta \left|\psi(\zeta)\right|^2 = 1 \text{ (e).} \tag{3}$$

It is easy to see that dimensionless electric field at the interface $GaAs/Al_xGa_{1-x}As$ is defined as $\Phi'(1/2) = \lambda_e^{2D}/2$ (this parameter is important for consideration of electrostatics in the barrier).

Thus, at a given electron concentration n_e^{2D}, we can completely solve the electrostatic and quantum-mechanic problems inside this QW, in particular to determine the position of quantization levels, spatial dependences of both wave function and potential profile.

2.2. Electrostatics of the barrier layer

Let two donor-doped δ-layers are placed at the distance $\pm d_i$ from the middle of QW. The impurity concentration in each δ-layer is assumed to be N_i. The donor concentration is supposed to be so large that wave functions of localized electrons in the donor states are overlapped and conductive channels are formed in the barriers. In $Al_xGa_{1-x}As$, the impurities of Si are shallow donors, as it was reported in the ref. [25]. For example, for the donor states with the energy 15 meV the electron localization radius a_H is close to 5 nm. Therefore, the criteria of Mott transition $N_i^{1/2} a_H \geq 0.35$ (see ref. [26]) can be fulfilled at $N_i > 5 \cdot 10^{11} \text{cm}^{-2}$. Moreover, at sufficient electron heating by the applied electric fields (see Section 4), the major part of electrons can transfer from the donor states to the conduction band.

Thus, one can assume that a positive charge of ionized impurity layer creates the electrostatic potential well for three-dimensional free electrons in the barrier layer. The electrostatic potential in the barrier region ($z > d/2$) has to satisfy the Poisson equation written as follows:

$$\frac{d^2\phi(z)}{dz^2} = \frac{4\pi e}{\kappa_0}\left[n_e^{3D}(z) - N_i\,\delta(z - d_i)\right] \qquad (4)$$

with three-dimensional concentration of electrons in the barrier $n_e^{3D}(z)$. According to the symmetry of the heterostructure under the consideration, it is sufficient to solve the electrostatic problem for $z > 0$. The estimations carried out bellow show that the effect of the electron quantization inside SWs is insignificant, and therefore, electrons can be treated as the three-dimensional ones. Indeed, SWs formed in the barrier are wide and shallow, meanwhile, electrons localized there have very low mobilities and very short relaxation times, which leads to the essential broadening of the levels. Assuming that electrons are nondegenerate and obey the Maxwell-Boltzmann statistics, we can write that

$$n_e^{3D}(z) = \frac{\left(2\pi m_b^* k_B T_e\right)^{3/2}}{4\pi^3\hbar^3} \exp\left[\left(E_F + e\phi(z)\right)/k_B T_e\right], \qquad (5)$$

where m_b^* and T_e is the effective mass of electrons and electron temperature in Γ-valley of $Al_xGa_{1-x}As$, respectively. Fermi level E_F is measured from the bottom of the unperturbed conduction band of barrier material and is constant across the entire heterostructure. Note, the distribution function (5) assumes that the drift velocity in the region of SW is small.

It is convenient to rewrite Eqs. (4) and (5) in the form of the dimensionless equations as follows:

$$\Phi^{\mp''} = \lambda_e^{3D}\,\theta_e^{3/2} \exp\left(\xi_F/\theta_e\right) \exp\left(\Phi^{\mp}/\theta_e\right). \qquad (6)$$

In the latter, signs "–" and "+" correspond to the spatial regions $1/2 \leq \zeta \leq D_i$ ($D_i = d_i/d$) and $\zeta \geq D_i$, respectively, $\theta_e = T_e/T$, $\xi_F = E_F/k_B T$ and dimensionless screening parameter $\lambda_e^{3D} = e^2 d^2 \left(2m_b^*\right)^{3/2} (k_B T)^{1/2} / \kappa_0 \pi^{1/2} \hbar^3$. The solutions of Eq. (6) have to satisfy the following boundary conditions:

$$\begin{aligned}
&\Phi^-(1/2) = 0 \quad (a),\\
&\Phi'^-(1/2) = \lambda_e^{2D}/2 \quad (b),\\
&\Phi^-(D_i) = \Phi^+(D_i) \equiv \Phi_i \quad (c),\\
&\Phi'^-(D_i) - \Phi'^+(D_i) = \lambda_i \quad (d),
\end{aligned} \qquad (7)$$

where $\lambda_i = 4\pi e^2 dN_i / \kappa_0 k_B T$ and Φ_i is the electrostatic potential corresponding to the bottom of the side well. Here, the condition (a) follows from the reference system of potential energy, and condition (b) is the result of continuity of the electric field at the interface $GaAs/Al_xGa_{1-x}As$. The conditions (c) and (d) express the continuity and discontinuity of the potential and electric field, respectively, in the point of the impurity δ-layer. Using (7), solutions of (6) can be found in the form of the implicit functions. In the region $1/2 \leq \zeta \leq D_i$,

$$\begin{aligned}
&\Phi'^- = \sqrt{\left(\lambda_e^{2D}/2\right)^2 + G(\theta_e, \xi_F) \times [\exp(\Phi^-/\theta_e) - 1]},\\
&\zeta = 1/2 + \int_0^{\Phi^-} \frac{d\Phi}{\sqrt{\left(\lambda_e^{2D}/2\right)^2 + G(\theta_e, \xi_F) \times [\exp(\Phi/\theta_e) - 1]}}.
\end{aligned} \qquad (8)$$

In the region $\zeta \geq D_i$,

$$\begin{aligned}
&\Phi'^+ = -\sqrt{G(\theta_e, \xi_F)} \exp\left(\Phi^+/2\theta_e\right),\\
&\Phi^+ = -2\theta_e \log\left[\exp\left(-\Phi_i/2\theta_e\right) + \right.\\
&\left.\sqrt{G(\theta_e, \xi_F)}/2\theta_e \times (\zeta - D_i)\right].
\end{aligned} \qquad (9)$$

Here $G(\theta_e, \xi_F) = 2\lambda_e^{3D}\theta_e^{5/2} \exp\left(\xi_F/\theta_e\right)$, Φ_i is the function of the electron temperature and Fermi level and is defined as follows:

$$\Phi_i(\theta_e, \xi_F) = 2\theta_e \times \log\left[\left(\lambda_i^2 - (\lambda_e^{2D}/2)^2 + G(\theta_e, \xi_F)\right) / 2\lambda_i \sqrt{G(\theta_e, \xi_F)}\right].$$

Note that solutions (9) far from the δ-layer are $\Phi^{+}(\infty) = -\infty$ and $\Phi^{'+}(\infty) = 0$. Finally, from the second equation of (8), we can obtain the following relationship between θ_e and ξ_F:

$$D_i = 1/2 + \int_0^{\Phi_i(\theta_e,\xi_F)} \frac{d\Phi}{\sqrt{\left(\lambda_e^{2D}/2\right)^2 + G(\theta_e,\xi_F)\times\left[\exp(\Phi/\theta_e)-1\right]}}. \quad (10)$$

Thus, at the given electron concentration n_e^{2D} in QW, one can able to solve the electrostatic problem completely, if we determine one of the parameters θ_e or ξ_F. For this purpose, it is necessary to consider electron transport in the quantum well and specify mechanisms of carrier exchange between QW and this barrier. Within the frames of simple consideration of the RST effect, we suppose that due to the strong electron-electron interaction there is a temperature balance between 2D electrons in QW and 3D electrons in SW. Under this assumption, the common electron temperature and Fermi level between these two groups of electrons are established even for non-equilibrium electron gas in QW.

3. Transport model for 2DEG in QW

As known, the basic electric characteristics of hot electrons are determined by non-equilibrium distribution function $f(\vec{p})$, where $\vec{p}$ is the electron momentum. In the frameworks of the classical kinetic theory, the distribution function is given by solution of Boltzmann transport equation, which in the case of steady-state and spatially uniform applied electric field $\vec{F}$ can be written as

$$-e\vec{F}\frac{\partial f(\vec{p})}{\partial \vec{p}} = I_{e-e}\{f\} + I_{lat}\{f\}, \quad (11)$$

where $I_{e-e}\{f\}$ is the collision integral of the electron-electron (e-e) scattering, and the collision integral $I_{lat}\{f\}$ describes the electron scattering by phonons and crystal lattice imperfections. As mentioned above, we consider the case of a high electron concentration, so that e-e collisions dominate over all the scattering process, and the electron subsystem is characterized by collective momentum and energy budget. Thus, to solve the kinetic equation (11), we can use the electron temperature approach with the distribution function taken in the form of shifted Fermi-Dirac distribution [27]

$$f(\vec{p},t) = \frac{1}{1+\exp\left\{\left[\varepsilon_\Gamma(\vec{p}) + E_1 - E_F - \vec{v}_d\vec{p}\right]/k_B T_e\right\}} \quad (12)$$

with $\varepsilon_\Gamma(\vec{p}) = p^2/2m^*$ and three unknown parameters: Fermi level E_F, drift velocity V_d and electron temperature T_e. The parameters E_F, T_e and V_d are to be found from the concentration, momentum and energy conservation equations that can be obtained by multiplying Eq. (11) by 1, p_x and p^2, respectively, followed by integrating them over all $\vec{p}$ (in our case, $\vec{p}$ is the two-dimensional vector). The similar approach of the solution of Boltzmann transport equation was applied at the analysis of the hot-electron kinetics in the bulk-like GaN [28]. In our case, these equations are

$$\begin{cases} n_e^{2D} = \overline{Q}_N\left(\overline{v}_d, \overline{\theta}_e, \overline{\xi}_F\right), \\ \overline{F} = \overline{Q}_P\left(\overline{v}_d, \overline{\theta}_e, \overline{\xi}_F\right), \\ \overline{F}\overline{v}_d = \overline{Q}_E\left(\overline{v}_d, \overline{\theta}_e, \overline{\xi}_F\right), \end{cases} \quad (13)$$

where the specific form of $\overline{Q}_N$ is determined only by the form of distribution function (12). The determination of the functions $\overline{Q}_P$ and $\overline{Q}_E$ already requires the specification of scattering mechanisms. Since, we mainly focus on the investigations of electron transport within the range of high fields in polar material, then the main dominant scattering mechanism that should be considered is the electron scattering by polar-optical phonons (for 2D electrons, it will be confinement phonons). Therefore, all dimensionless parameters in the system (13) are written through the inherent parameters for the optical phonon scattering (see Appendix). We describe other possible electron scattering (acoustic phonons, roughness, dislocations) that can be important in the low-field range, introducing the single elastic and isotropic scattering mechanism with an effective momentum relaxation time τ_p. The latter value corresponds to the typical transport time of the low-field mobility in these heterostructures [23]. The explicit forms of the functions $\overline{Q}_{N,P,E}$ are given in Appendix.

Thus, four non-linear equations (10) and (13) allow us to completely solve the steady-state problem of RST. In particular, at the given electron concentration n_e^{2D}, we can find the drift velocity, electron temperature, position of the Fermi level and corresponding value of applied electric field. Having these characteristics, we can reproduce the electrostatic potential profile (Eqs. (8) and (9)) and concentration profile (Eq. (5)) in the barrier layer.

Finally, we need to shortly discuss electron transport in impurity SWs. As mentioned above, electrons inside SWs have low mobilities due to the strong scattering by impurities, dislocations and optical phonons at high temperatures. The typical values of electron mobilities in SW μ_{SW} are the order of few hundreds cm^2/V·s [19, 23]. It allows us to use Ohm's law for the current flowing through SWs. The total current is a sum of currents flowing in QW and SWs:

$$J_{tot} \equiv J_{QW} + J_{SW} = en_e^{2D}(F)\,v_d(F) + 2e\left\langle n_e^{3D}(F)\right\rangle_z \mu_{SW}F, \quad (14)$$

where the factor 2 takes into account left and right symmetric SWs, and $\left\langle n_e^{3D} \right\rangle_z = \int_d^\infty n_e^{3D} dz$ is the total two-dimensional electron concentration in SW. Accordingly, the charge conservation law looks as $2\left\langle n_e^{3D} \right\rangle_z = 2N_i - n_e^{2D}$.

4. Results and discussion of steady-state problem

Now, let us apply the model of RST and the procedure of calculations described in Sections 2 and 3 to heterostructures $Al_xGa_{1-x}As/GaAs/Al_xGa_{1-x}As$ with parameters characteristic to those of the experimental samples studied in the ref. [23]. In calculations, we will use the following approximation for barrier height V_b = $1.155x + 0.37x^2$ (in eV) and the effective mass $m_b^* = (0.063 + 0.083x)\, m_0$ (m_0 is the free electron mass) [29]. At the beginning, it is useful to estimate the range of values of *d* and *x*, where the single energy level model for electrons in QW can be applied.

Two curves in Fig. 1 that are calculated for unperturbed conduction band structure under the condition (3(a)) bound four regions of parameters *x* and *d*, where four different cases are realized. The region I corresponds to the frameworks of the presented model – there is the only one discrete level Γ_1 in QW. Other regions correspond to the parameters of the heterostructure, when several energy levels corresponding to the minima of Γ_1 and satellite L-valleys can exist in QW. For example, two discrete levels of Γ_1 and L_1 (region II), two discrete levels of Γ_1 and Γ_2 (region III) and three discrete levels of Γ_1, Γ_2 and L_1 (region IV) are in QW. Below, calculations are presented for the following parameters: $x = 0.2$ and $d = 12$ nm at which the role of the upper levels of size quantization can be neglected.

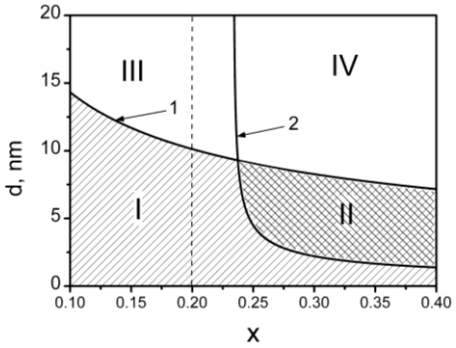

Fig. 1. The QW width vs alloy composition. Curve *1* found from the equation $V_b(x) = 2\hbar^2\pi^2/m_\Gamma^* d^2$ (condition when the second level, Γ_2, of Γ valley coincides with hight of barrier). Curve *2* found from the equation $V_b(x) = \Delta_{\Gamma L} + \hbar^2\pi^2/2m_L^* d^2$ (condition when the first level L_1 of *L* valley coincides with the barrier hight), where $m_L^* = 0.85m_0$ and $\Delta_{\Gamma L} = 0.29$ eV are the effective mass of density of states for *L* valley and energy separation between Γ and *L* valleys for GaAs (see ref. [29]), respectively.

Figs 2 and 3 provide the results of calculation of the field dependences of transport characteristics and spatial distributions of the electrostatic potential energy and electron concentration.

As seen, the current-voltage characteristic of the heterostructure $J_{tot}(F)$ roughly consists of several intervals with distinct behavior. The linear behavior (Ohm's law) is observed in the range of weak applied fields of <0.1 kV/cm. In this case, the values of n_e^{2D} and T_e are close to its equilibrium values. Note, at the equilibrium conditions, $n_e^{2D} = 1.85 \times N_i$, i.e. approximately 92% of all electrons are transferred from both SWs to QW. Within the range of applied fields 0.1 to 1 kV/cm, both $J_{tot}(F)$ and $v_d(F)$ have a sublinear behavior, which can be explained by activation of the electron-optical-phonon scattering mechanism. However, in this range the effect of RST is still inconspicuous, the electron concentration in QW is decreased only by ≈8%. Starting from the field of 1 kV/cm, the effect of RST begins to develop, which results in quasi-saturated behavior of the current-voltage characteristic $J_{tot}(F)$. At the same time, the current-voltage characteristics that neglects the RST effect shows a superlinear growth. Within the range 1 to 2 kV/cm, electrons in QW gain significant heating, electron temperature is increased from 150 up to 350 K, as a result the electron concentration in QW decreases from 1.7 down to $1.3N_i$ (25-% decrease). At fields above the threshold field, $F \approx 2$ kV/cm, the well-developed effect of RST leads to the dropping current-voltage characteristic.

The similar value of threshold field was reported by Hess and co-workers in ref.[20, 21] where the electron transport in the AlGaAs/GaAs/AlGaAs structure was studied by both numerical and analytical methods. In contrast of the presented paper, those investigations relate to the wide heterostructures ($d_{GaAs} \approx 40$ nm), for which the electron transport inside GaAs layer was treated as the three-dimensional one.

Theoretical predictions of the emergence of current-voltage characteristics with a negative differential resistance (NDR) are the main results of the study of RST effect in heterostructures. In principle, physics of appearance of NDR under RST and Gunn effects are similar. In the Gunn effect, electrons transfer from one valley of high mobility to another of low mobility in momentum space. The most important distinction is the fact that RST-effect device can be controlled to a greater degree than with a device based on the Gunn effect. The Gunn effect has the intervalley deformation potential as a driven parameter, which is a material property and cannot be changed. In the case of the RST-effect device, the driven parameters are the mobility of the $Al_xGa_{1-x}As$ layer and height of barriers, which can be controlled by adjusting the doping of the layers and chemical composition *x*.

Semiconductor Physics, Quantum Electronics & Optoelectronics, 2015. V. 18, N 1. P. 1-11.
doi: 10.15407/ spqeo18.01.001

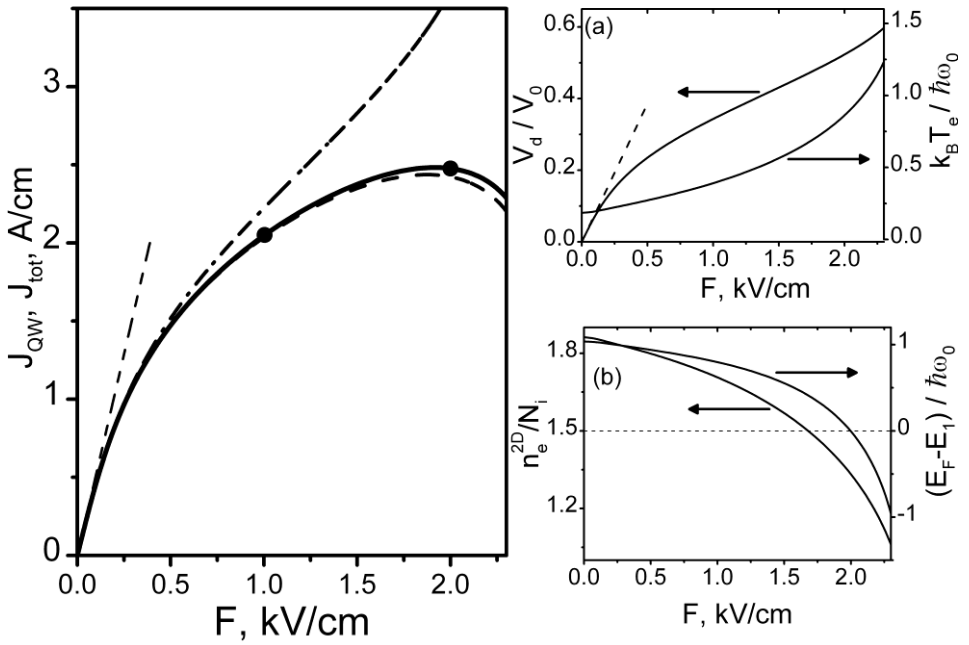

Fig. 2. Main panel: solid and dashed lines are the current-voltage characteristics $J_{tot}(F)$ and $J_{QW}(F)$, respectively. Dash-dotted line is the current J_{QW} calculated neglecting the RST effect for the concentration $n_e^{2D} = 1.85N_i$. Panel (a) shows the field dependences of the electron temperature $T_e(F)$ and the drift velocity $V_d(F)$. Panel (b) shows the field dependences $n_e^{2D}(F)$ and Fermi level $E_F(F)$. Parameters of the heterostructure are following: impurity concentration $N_i = 5\cdot10^{11}$ cm^{-2}, position $d_i =$ 24 nm, mobility in SW $\mu_{SW} = 500$ cm^2/V·s and ambient temperature $T = 77$ K. Optical phonon energy, $\hbar\omega_0 = 36$ meV and characteristic velocity, $V_0 = 4.4\cdot10^7$ cm/s. Ohmic dependence shown in panel (a) corresponds to the mobility $\approx 3\cdot10^4$ cm^2/V·s (momentum relaxation time $\tau_p = 1.5$ ps).

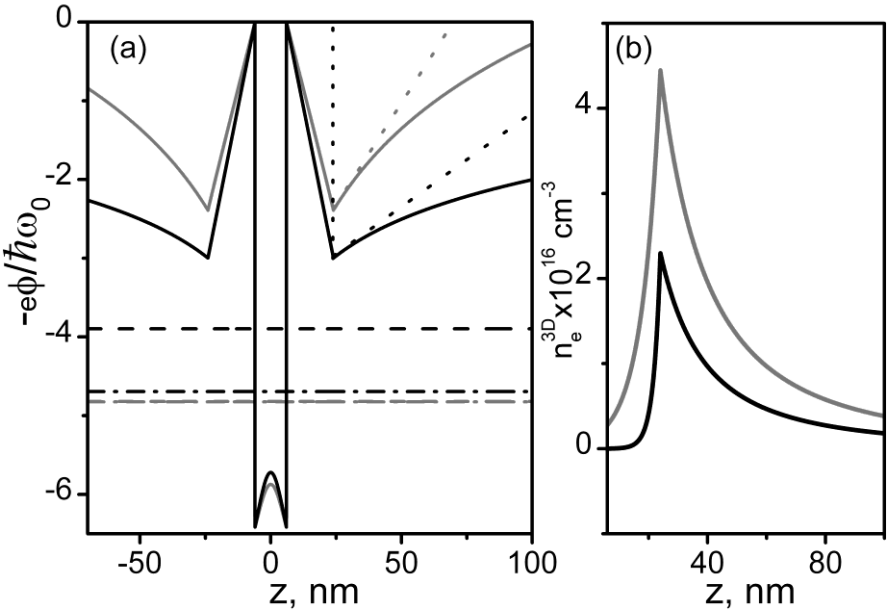

Fig. 3. Potential energy profiles $-e\phi(z)$ (panel a) and electron concentration profile $n_e^{3D}(z)$ (panel b). Black and grey lines correspond to the $F = 1$ kV/cm and 2 kV/cm, respectively (these fields are marked by points in the characteristics $J_{tot}(F)$ in Fig. 2. Dashed and dash-dotted lines depict the positions of the Fermi level and first level of size quantization, respectively.

Semiconductor Physics, Quantum Electronics & Optoelectronics, 2015. V. 18, N 1. P. 1-11.
doi: 10.15407/ spqeo18.01.001

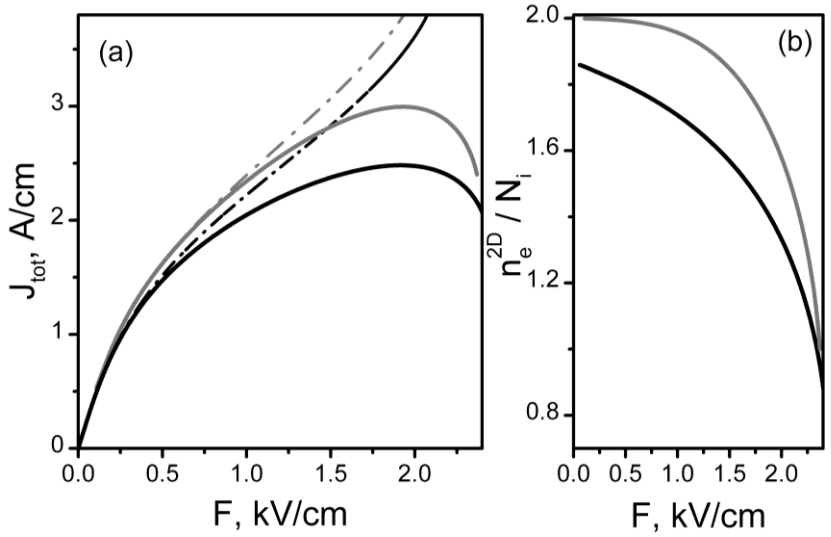

Fig. 4. Dependences of $J_{tot}(F)$ (panel a) and $n_e^{2D}(F)$ (panel b). Black and grey lines correspond to d_i = 24 nm and 12 nm, respectively, T = 77 K. Dash-dotted lines are the currents J_{OW} without RST.

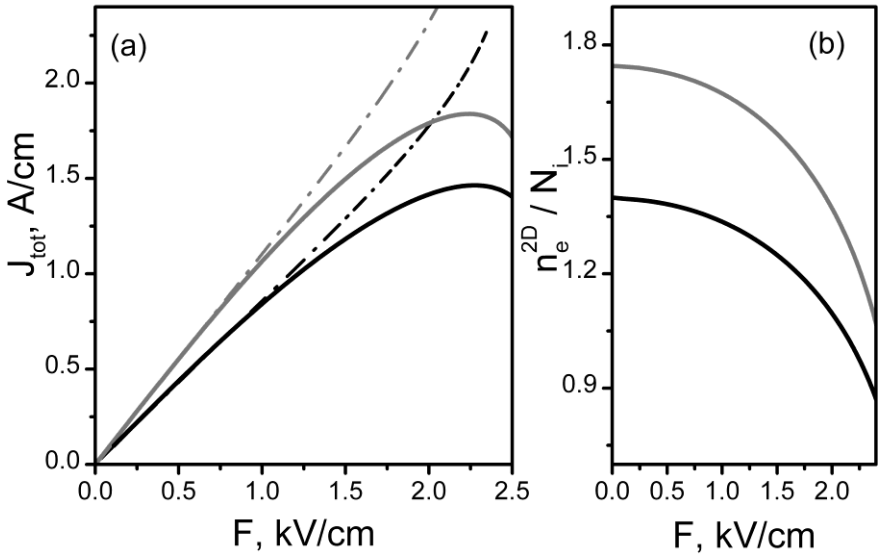

Fig. 5. The same as in Fig. 4 for T = 300 K.

The profiles of potential energy and electron concentration in the barriers are illustrated in Figs. 3a and 3b, respectively, for two characteristic fields F = 1 kV/cm and 2 kV/cm. One of them is the field of the onset of RST, and the second one is the threshold field, respectively. As seen, the position of the quantization level inside QW weakly depends on the amplitudes of the applied field. The values of E_1 are practically the same for both fields and approximately equal to –0.17 eV ($-4.75\hbar\omega_0$). However, the position of Fermi levels is appreciably changed with F. For example, at F = 1 kV/cm, the electron gas is degenerated, the Fermi level is equal to –0.14 eV ($-3.89\hbar\omega_0$) and lies above the quantization level. At F = 2 kV/cm, $E_F \approx E_1$, and the electron gas has intermediate degeneracy.

In the barrier, the positive impurity charge and negative electron charge form the macroscopic electrostatic wells with an asymmetric profile. The bottoms of SWs correspond to the position of δ-layer. With an increase of the applied field and, consequently, with increasing the electron population inside the barrier regions, the bottoms of SWs are lifted up, and SWs become shallower. In the limiting case, when all electrons from QW transfer to the barriers, the macroscopic electrostatic potential given by Poisson equation (4) is equal to zero, and the resulting

profile of the heterostructure will be rectangular. In the opposite limiting case, when all electrons transfer from the barriers to QW, the resulting electrostatic profile in the barrier region will be like to the double charge layer. Within the region $1/2 < \zeta < D_i$, the potential energy has a linear spatial dependence $\Phi(\zeta) = -\lambda_e^{2D}/2\times\zeta$ and in the region $\zeta > D_i$, the potential energy is constant, $\Phi(\zeta) = \Phi_i = -\lambda_e^{2D}/2\times D_i$, and electron confinement disappears.

As shown in Fig. 3b, the profiles of electron concentration also have an asymmetric form in compliance with the potential profile of SWs. The maximum of electron concentration is reached at the $z = d_i$, and electrons are more strongly localized in the direction of QW than in the direction of a depth of the barrier. So, at z = 20 nm (at –5 nm away from d_i) the electron concentration is decreased almost by one order. The same reduction occurs at $z >$ 120 nm (+100 nm away from d_i).

For the obtained electrostatic profiles in the barrier, it is still necessary to check the possibility of electron quantization. The estimations can be easy carried out by modeling triangular well with the potential profile: $V(z) = eF_z z$ at $z > d_i$ and $V = \infty$ for $z < d_i$ (shown in Fig. 3a with the dots). For the parameters of $Al_{0.2}Ga_{0.8}As$, the values of energy levels $E_{n,b}$ are given by the simple formula $E_{n,b} = 1.68\cdot10^{-5} p_n F_z^{2/3}$ (see, for example, the ref. [30]), where p_n is zeros of the Airy functions. Here, energies are given in units of eV and F_z – in V/cm. For the potential well depicted by the black dots, $F_z = 10^4$ V/cm (lateral field F = 1 kV/cm) as a result the first three levels with respect to the bottom of the well are equal to 0.5, 0.88, 1.2 in the units of $\hbar\omega_0$. For the potential well depicted by the grey dots, $F_z = 2\cdot10^4$ V/cm (lateral field F = 2 kV/cm), as a result, the first three levels are equal to 0.8, 1.4, 1.2 in the same units. As seen, for both cases the inter-level distances are of the order of $0.5\hbar\omega_0$ (≈0.02 eV), which is comparable with the values of the electron temperatures. Taking into account that the inter-level distance for the original potential wells will be even less, the quantization effect for electrons in electrostatic SWs can be neglected. Thus, the presented model of electron transport in the heterostructure with δ-doped barriers is applicable.

Let us briefly analyze the effect of RST at other parameters. Figs. 4 and 5 present the comparison of current-voltage characteristics and field dependences of electron population inside QW for two different positions of the δ-doped layer d_i = 12 nm and 24 nm, as well as two different temperatures T = 77 K and 300 K.

As seen, the population of QW is increased with decreasing the distance between QW and δ-layer. Under the equilibrium conditions, in the case of heterostructure with d_i = 12 nm (grey curve in Fig. 4b), almost 100% of electrons transfer from the barriers to QW. Note that in the range of sub-threshold fields, 0 to 2 kV/cm, QW in the heterostructure with smaller d_i has a greater population (grey curve lies above black curve). However, at fields above the threshold, QW in the heterostructure with lower d_i is depopulated more rapidly. It reflects in behavior of the current-voltage characteristics: currents obtained for the heterostructure with d_i = 12 nm exceed those obtained for the heterostructure with d_i = 24 nm. The threshold fields for both heterostructures are practically the same (2 kV/cm). At the fields above threshold, the current is more sharply decreased for d_i = 12 nm than for d_i = 24 nm.

At room temperature (see Fig. 5), general behavior of the dependences $J_{tot}(F)$ and $n_e^{2D}(F)$ are modified as compared with the case of nitrogen temperature. In particular, the high-temperature current-voltage characteristic has a wider interval of the ohmic behavior 0 to 1.5 kV/cm, and the threshold field is increased up to the value 2.3 kV/cm.

Under equilibrium conditions, the same structure at T = 300 K and 77 K has different populations of QW, and they are equal to $n_e^{2D} = 1.4\cdot N_i$ and $1.84\cdot N_i$, respectively (black curves in Figs. 5b and 4b). Moreover, within the range of applied fields 0 to 2 kV/cm, electron redistribution between QW and SWs is less at the ambient temperature T = 300 K than at 77 K. For example, at T = 77 K, n_e^{2D} varies from 1.85 to $1.33\cdot N_i$, which is 25% from the initial value, and at T = 300 K, n_e^{2D} varies from 1.4 to $1.09\cdot N_i$, which is only 18% from the initial value.

It can be explained by the two following reasons. First one is associated with different temperature dependences of the density of states for three-dimensional and two-dimensional electrons. For 3D electrons, the density of states is proportional to $T_e^{3/2}$

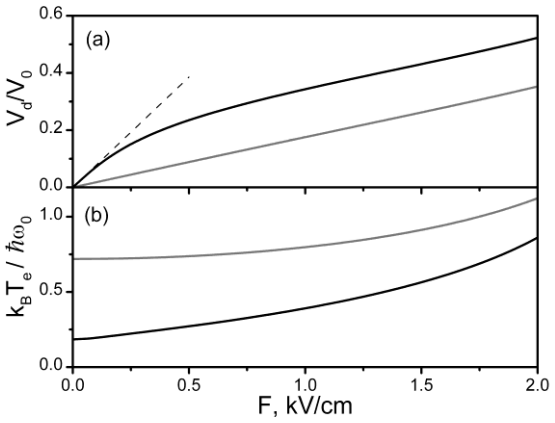

Fig. 6. Dependences of $V_d(F)$ (panel a) and $T_e(F)$ (panel b) for the 2D electron gas inside QW. Black and grey curves correspond to the temperatures 77 and 300 K, respectively. The calculated values of low-field mobility are $3\cdot10^4$ and $8\cdot10^3$ cm^2/V·s at T = 77 and 300 K, respectively. Other parameters of the heterostructure are the same as in Fig. 2.

and increases with temperature more rapidly than for 2D electrons, which is proportional to T_e. The second reason is decreasing the electron mobility in QW due to activation of electron scattering by polar optical phonons. It proves the field dependences of $T_e(F)$ and $V_d(F)$ that are obtained for the cases of room and nitrogen temperatures (see Fig. 6).

5. Summary

In the conclusion, it has been developed the theory of the real-space transfer effect in heterostructures $Al_xGa_{1-x}As/GaAs/Al_xGa_{1-x}As$ with narrow quantum wells (close to 10 nm) and δ-doped barriers. Under the assumption of the fast carrier exchange between well and barrier layers, the field dependences of electron population in the quantum well, the Fermi level and current-voltage characteristics were obtained. It has been ascertained that, for the heterostructure with $x = 2$ and doping of $5\cdot10^{11}\text{cm}^{-2}$, the RST effect is well pronounced at the applied electric fields larger than 1 kV/cm. Within the interval of fields 1 to 2 kV/cm, essential depopulation of QW with a variation of the Fermi level occurs, which leads to saturation of current-voltage characteristics. These results qualitatively explain the measured non-linear current-voltage characteristics of the heterostructures experimentally studied in the paper [23]. It should be noted that the RST effect can be also detected in the electro-optical experiments. For example, variation of the Fermi level by applied electric field can be directly observed in the optical absorption edge measurements through detecting the Burstein-Moss shift [31].

Under the fields higher than 2 kV/cm, the well-developed effect of RST can lead to the emergence of negative differential resistance. Moreover, NDR effect can exist at both nitrogen and room temperatures. The obtained results allow to suggest that heterostructure $Al_xGa_{1-x}As/GaAs/Al_xGa_{1-x}As$ with δ-doped barriers can be used for desirable current control in different devices.

Acknowledgement

The work has been carried out in the framework of the State Program "Nanotechnology and nanomaterials" (2010–2014), project №1.1.7.18/14-M. The author acknowledges the support by The State Fund for Fundamental Researches (Grant F53.2/031). Also, the author is sincerely grateful to Prof. V.A. Kochelap and Dr. V.N. Poroshin for their interest and active discussion of various aspects of this work.

Appendix: Summary of balance integrals

In the case of the degenerate 2DEG, the scattering integrals are the bilinear functional in respect to the distribution function:

$$I_{op} = \frac{S}{(2\pi\hbar)^2}\int d\,\vec{p}\,' W_{op}(\vec{p}\,',\vec{p}) f(\vec{p}\,')\times \\ \times\left[1- f(\vec{p})\right] - W_{op}(\vec{p},\vec{p}\,') f(\vec{p})\left[1- f(\vec{p}\,')\right]. \tag{15}$$

Here, $\vec{p}$ is the longitudinal electron momentum. For the intravalley electron scattering process by the confinement optical phonon, the scattering probability is given by [30]

$$W_{op}(\vec{p}\,',\vec{p}) = W^{+}_{op}(\vec{p}\,',\vec{p}) + W^{-}_{op}(\vec{p}\,',\vec{p}),$$
$$W^{\pm}_{op}(\vec{p}\,',\vec{p}) = \frac{8\pi^2\hbar^2\omega_0 e^2}{V}\left(\frac{1}{\kappa_\infty}-\frac{1}{\kappa_0}\right)\left(N_0+\frac{1}{2}\pm\frac{1}{2}\right)\times \\ \times\sum_{k=1}^{\infty} G_k^2\,\frac{\delta\left(\varepsilon_\Gamma(\vec{p}\,')-\varepsilon_\Gamma(\vec{p})\mp\hbar\omega_0\right)}{(\vec{p}\,'-\vec{p})^2-(\pi\hbar k/d)^2}, \tag{16}$$

where superscripts "+" and "–" correspond to the optical phonon emission an absorption processes, respectively, ω_0 is the optical phonon frequency, $N_0 = \left(\exp(\eta_0)-1\right)^{-1}$ expresses the equilibrium phonon distribution function with $\eta_0 = \hbar\omega_0/k_BT$ (effects of the phonon heating are neglected); κ_∞ and κ_0 are the high-frequency and low-frequency permittivities, and $G_k = 8/\left(\pi k(k^2-4)\right)$ is the form-factor with an odd k, which numerates the modes of confinement optical phonons. Note, probability (16) is written for rectangular infinitely-deep quantum well and takes into account only the lowest subband of size quantization.

Following the procedure described in Section (3) and using explicit expression (16), the momentum and energy balance integrals take the forms:

$$Q_P^{op} = -\frac{P_0^3}{4\tau_0}\sum_{k=1}^{\infty}G_k^2\left[\begin{array}{l}\displaystyle\int_0^\infty dx\int_{-\pi}^{\pi}d\phi\,\frac{(N_0+1)\cos(\phi)\,f(x+1,\phi)\,r_k^-}{\sqrt{x+1}}+\frac{N_0\,f(x,\phi)\cos(\phi)\,r_k^+}{\sqrt{x}}- \\ \displaystyle-\frac{1}{\pi}\int_0^\infty dx\int_{-\pi}^{\pi}d\phi\int_{-\pi}^{\pi}d\phi'\,\frac{\left(\sqrt{x+1}\cos(\phi')-\sqrt{x}\cos(\phi)\right)f(x+1,\phi')f(x,\phi)}{a_k+b_k\cos(\phi+\phi')}\end{array}\right], \tag{17}$$

$$Q_E^{op} = -\frac{P_0^4}{2\tau_0}\sum_{k=1}^{\infty}G_k^2\left[\begin{array}{l}\displaystyle\int_0^\infty dx\int_{-\pi}^{\pi}d\phi\,\frac{(N_0+1)\,f(x+1,\phi)-N_0\,f(x,\phi)}{\sqrt{a_k^2-b_k^2}}- \\ \displaystyle-\frac{1}{2\pi}\int_0^\infty dx\int_{-\pi}^{\pi}d\phi\int_{-\pi}^{\pi}d\phi'\,\frac{f(x+1,\phi')f(x,\phi)}{a_k+b_k\cos(\phi+\phi')}\end{array}\right]. \tag{18}$$

In the latter, $\tau_0 = \left[2\pi e^2/\hbar d\cdot\left(1/\kappa_\infty - 1/\kappa_0\right)\right]^{-1}$ defines the characteristic electron-optical phonon scattering time, $P_0 = \sqrt{2m^*\hbar\omega_0}$ is the characteristic electron momentum corresponding to the optical phonon energy $\hbar\omega_0$. The introduced variables a_k, b_k and $r_k^{\pm}$ are the functions of dimensionless energies, $x = \varepsilon_\Gamma/\hbar\omega_0$, $x_k = (\pi\hbar k/dP_0)^2$ and they are determined as follows: $a_k = 2x+1+x_k$, $b_k = 2\sqrt{(x+1)x}$ and $r_k^{\pm} = 1-\left(x_k \pm 1\right)\Big/\sqrt{a_k^2 - b_k^2}$. The distribution function

$$f(x,\phi) = \frac{1}{1+\exp\left[\left\{x - \bar{\xi}_F - 2\bar{v}_d\sqrt{x}\cos(\phi)\right\}/\bar{\theta}_e\right]} \qquad (19)$$

is rewritten in the dimensionless variables (x,ϕ), where ϕ is the angle between the electron momentum and the drift velocity. Other dimensionless parameters are: $\bar{v}_d = m^*V_d/P_0$, $\bar{\theta}_e = k_B T_e/\hbar\omega_0$, $\bar{\xi}_F = \left(E_F - E_1\right)/\hbar\omega_0$.

In the case of non-degenerate electron gas, the balance integrals (17), (18) are essentially simplified:

$$Q_P^{op} = -\frac{\pi P_0^3}{2\tau_0}\exp\left(\bar{\xi}_F/\bar{\theta}_e\right)\times$$
$$\times\sum_{k=1}^{\infty}G_k^2\left[\int_0^{\infty}dx\frac{(N_0+1)\exp\left(-(x+1)/\bar{\theta}_e\right)I_1\left(2\bar{v}_d\sqrt{x+1}/\bar{\theta}_e\right)r_k^-}{\sqrt{x+1}} + \frac{N_0\exp\left(-x/\bar{\theta}_e\right)I_1\left(2\bar{v}_d\sqrt{x}/\bar{\theta}_e\right)r_k^+}{\sqrt{x}}\right],$$

$$Q_E^{op} = -\frac{\pi P_0^4}{\tau_0}\exp\left(\bar{\xi}_F/\bar{\theta}_e\right)\times$$
$$\times\sum_{k=1}^{\infty}G_k^2\left[\int_0^{\infty}\frac{(N_0+1)\exp\left(-(x+1)/\bar{\theta}_e\right)I_0\left(2\bar{v}_d\sqrt{x+1}/\bar{\theta}_e\right)}{\sqrt{a_k^2-b_k^2}} - \frac{N_0\exp\left(-x/\bar{\theta}_e\right)I_0\left(2\bar{v}_d\sqrt{x}/\theta_e\right)}{\sqrt{a_k^2-b_k^2}}\right], \qquad (20)$$

where $I_{0,1}$ denote the Bessel functions of the third kind.

In the simple case of the elastic and isotropic electron scattering, the balance integrals are reduced to the simple expressions: $Q_P^{el} = -(2\pi\hbar)^2 n_e^{2D}/2\times m_\Gamma^* v_d/\tau_p$ and $Q_E^{el} = 0$. The latter reflects the fact that electrons cannot dissipate their energy during the pure elastic scattering.

The momentum and energy balance integrals in dimensionless form introduced in the system (13) are:

$$\bar{Q}_P\left(\bar{v}_d,\bar{\theta}_e,\bar{\xi}_F\right) = -\frac{2}{(2\pi\hbar)^2 n_e^{2D}}\frac{\tau_0}{P_0}Q_P^{op} + \bar{v}_d/\bar{\tau}_p,$$

$$\bar{Q}_E\left(\bar{v}_d,\bar{\theta}_e,\bar{\xi}_F\right) = -\frac{1}{(2\pi\hbar)^2 n_e^{2D}}\frac{\tau_0}{P_0^2}Q_E^{op},$$

where the dimensionless electric field is defined as $\bar{F} = -eF\tau_0/P_0$ and relaxation time $\bar{\tau}_p = \tau_p/\tau_0$. Finally, the balance integral $\bar{Q}_N\left(\bar{v}_d,\bar{\theta}_e,\bar{\xi}_F\right)$ is nothing but definition of the two-dimensional electron concentration, and for the distribution function (19) it has the form:

$$Q_N\left(\bar{v}_d,\bar{\theta}_e,\bar{\xi}_F\right) \equiv n_e^{2D} = \frac{P_0^2\bar{\theta}_e}{2\pi\hbar^2}\log\left[1+\exp\left(\left\{\bar{\xi}_F + \bar{v}_d^2\right\}/\bar{\theta}_e\right)\right].$$

References

1. W.T. Masselink, Electron velocity in GaAs: Bulk and selectively doped heterostructures // *Semicond. Sci. Technol.* **4**, p. 503-512 (1989).
2. S.J. Pearton, J.C. Zolper, R.J. Shul, and F. Ren, GaN: Processing, defects, and devices // *J. Appl. Phys.* **86**, p. 1 (1999).
3. O.J. Pooley, A.M. Gilbertson, P.D. Buckle, R.S. Hall, L. Buckle, M.T. Emeny, M. Fearn, L.F. Cohen and T. Ashley, Transport effects in remote-doped InSb/$Al_xIn_{1-x}Sb$ heterostructures // *New J. Phys.* **12**, p. 053022 (2010).
4. H. Sun, A.R. Alt, H. Benedickter, E. Feltin, J.-F. Carlin, M. Gonschorek, N.R. Grandjean, and C.R. Bolognesi, 205-GHz (Al,In)N/GaN HEMTs // *IEEE Electron Dev. Lett.* **31**(9), p. 957-959 (2010).
5. K. Sakai and M. Tani, *Terahertz Optoelectronics* (Topics in Applied Physics **97**, p. 1-31), Ed. K. Sakai. Springer, Berlin, 2005.
6. P.H. Siegel, THz technology // *IEEE Trans. Microwave Theory and Tech*. **50**(3), p. 910-928 (2002).
7. L. Ardaravicius, A. Matulionis, J. Liberis, O. Kiprijanovic, M. Ramonas, L.F. Eastman, J.R. Shealy, and A. Vertiatchikh, Electron drift velocity in AlGaN/GaN channel at high electric fields // *Appl. Phys. Lett.* **83**(19), p. 4038-4040 (2003); V.V. Korotyeyev, V.A. Kochelap and K.W. Kim, Electron transport in bulk GaN under ultrashort high-electric field transient // *Semicond. Sci. Technol.* **26**, 105008 (2011).
8. B.A. Danilchenko, S.E. Zelensky, E. Drok, S.A. Vitusevich, S.V. Danylyuk, N. Klein, H. Luth, A.E. Belyaev, and V.A. Kochelap, Hot carrier energy losses in conducting layers of AlGaN/GaN hetero-structures grown on SiC and Al_2O_3 substrates // *phys. status solidi* (*b*), **243**(7), p. 1529-1532 (2006); Excess low-frequency noise in AlGaN/GaN-based high-electron-mobility transistors // *Appl. Phys. Lett.* **80**(12), p. 2126-2128 (2002).
9. O. Yilmazoglu, K. Mutamba, D. Pavlidis, T. Karaduman, First observation of bias oscillations in GaN Gunn diodes on GaN substrate // *IEEE Trans. Electron. Devices*, **55**(6), p. 1563-1567 (2008).

10. A. Lisauskas, A. Reklaitis, R. Venckevicius, I. Kasalynas, G. Valusis, G. Grigaliunaite-Vonseviciene, H. Maestre, J. Schmidt, V. Blank, M.D. Thomson, H.G. Roskos, and K. Kohler, Experi-mental demonstration of efficient pulsed terahertz emission from a stacked GaAs/AlGaAs p-i-n-i heterostructure // *Appl. Phys. Lett.* **98**, p. 091103 (2011).
11. W. Knap, J. Lusakowski, T. Parenty, S. Bollaert, A. Cappy, V.V. Popov and M.S. Shur, Terahertz emission by plasma waves in 60 nm gate high electron mobility transistors // *Appl. Phys. Lett.* **84**, p. 2331-2334 (2004).
12. M. Dyakonov and M. Shur, Current instability and plasma waves generation in ungated two-dimensional electron layers // *Appl. Phys. Lett.* **87**, p. 111501 (2005).
13. S. Spasov, G. Allison, A. Patane, L. Eaves, M.Yu. Tretyakov, A. Ignatov, M. Hopkinson, and G. Hill, High field electron dynamics in dilute nitride Ga(AsN) // *Appl. Phys. Lett.* **93**, p. 022111 (2008).
14. M. Asada, S. Suzuki, and N. Kishimoto, Resonant tunneling diodes for sub-terahertz and terahertz oscillators // *Jpn. J. Appl. Phys.* **47**(6), p. 4375-4384 (2008).
15. V.V. Korotyeyev, V.A. Kochelap, A.A. Klimov, K.W. Kim, D.L. Woolard, Tunable terahertz-frequency resonances and negative dynamic conductivity of two-dimensional electrons in group-III nitrides // *J. Appl. Phys.* **96**, p. 6488-6491 (2004).
16. V.V. Korotyeyev, V.A. Kochelap, A.A. Klimov, G. Sabatini, H. Marinchio, C. Palermo, and L. Varani, Theory of ballistic electron transport in n^+-i-n^+ diodes. Negative dynamic resistance in THz-frequency range // *J. Nanoelectron. Optoelectron*. **6**, p. 169-187 (2011).
17. Z.S. Gribnikov, Negative differential conductivity in a multilayer heterostructure // *Fizika, tekhnika poluprovod.* **6**, p. 1380-1382 (1972), in Russian.
18. W.T. Masselink, Real-space-transfer of electrons in InGaAs/InAlAs heterostructures // *Appl. Phys. Lett.* **67**, p. 801-803 (1995).
19. Z.S. Gribnikov, K. Hess and G.A. Kosinovsky, Nonlocal and nonlinear transport in semiconductors: Real-space transfer effects // *J. Appl. Phys.* **77**, p. 1337-1373 (1995).
20. T.H. Glisson, J.R. Hauser, M.A. Littlejohn, K. Hess, B.G. Streetman et al., Monte Carlo simulation of real space electron transfer in GaAs-AlGaAs heterostructures // *J. Appl. Phys.* **51**, p. 5445-5449 (1980).
21. H. Shichijo, K. Hess and B.G. Streetman, Real-space electron transfer by thermionic emission in GaAs–$Al_xGa_{1-x}As$ heterostructures: Analytical model for large widths // *Solid-State Electronics*, **23**, p. 817-822 (1980).
22. Ch.-K. Hahn, T. Sugaya, K-Y. Jang, X.-L. Wang and M. Ogura, Electron transport properties in a GaAs/AlGaAs quantum wire grown on V-grooved GaAs substrate by metal-organic vapor phase epitaxy // *Jpn. J. Appl. Phys.* **42**, p. 2399-2403 (2003).
23. V.V. Vainberg, A.S. Pylypchuk, V.N. Poroshin, O.G. Sarbey, Effects of the real-space transfer of charge carriers in n-AlGaAs/GaAs heterostructures with delta-layers of impurity in the barriers // *Ukr. J. Phys.* **59**(7), p. 721-725 (2014).
24. T. Laurent, R. Sharma, J. Torres, P. Nouvel, S. Blin, L. Varani, Y. Cordier, M. Chmielowska, S. Chenot, J.-P. Faurie, B. Beaumont, P. Shiktorov, E. Starikov, V. Gruzinskis, V.V. Korotyeyev, and V.A. Kochelap, Voltage-controlled sub-terahertz radiation transmission through GaN quantum well structure // *Appl. Phys. Lett.* **99**, p. 082101 (2011).
25. N. Chand, T. Henderson, J. Klem, W.T. Masselink, R. Fischer, Y.-Ch. Chang, and H. Morkoc, Comprehensive analysis of Si-doped $Al_xGa_{1-x}As$ (x = 0 to 1): Theory and experiments // *Phys. Rev. B*, **30**, p. 4481-92 (1984).
26. K. Schmalz, I.N. Yassievich, K.L. Wang, and S.G. Thomas, Localized-state band induced by δ-doping in Si/$Si_{1-x}Ge_x$/Si quantum wells // *Phys. Rev. B*, **57**, p. 6579 (1998).
27. V.E. Gantmakher and Y.B. Levinson, *Carrier Scattering in Metals and Semiconductors*. North-Holland, Amsterdam, 1987.
28. K.W. Kim, V.A. Kochelap, V.N. Sokolov, and S.M. Komirenko, Quasi-ballistic and overshoot transport in group III-nitrides in; *GaN-based Materials and Devices: Growth, Fabrication, Characterization and Performance*, ed. by M. Shur and R.F. Davis. World Scientific, 2004.
29. M. Levinstein, S. Rumyantsev and M. Shur, *Handbook Series on Semiconductor Parameters*, vol. 1, 2. World Scientific, London, 1996, 1999.
30. V.V. Mitin, V.A. Kochelap, and M. Stroscio, *Quantum Heterostructures for Microelectronics and Optoelectronics*. Cambridge University Press, New York, 1999.
31. H. Sakaki, H. Yoshimura and T. Matsusue, Carrier concentration dependent absorption spectra of modulation doped n-AlGaAs/GaAs quantum wells and performance analysis of optical modulators and switches using Carrier Induced Bleaching (CIB) and Refractive Index Change (CIRIC) // *Jpn. J. Appl. Phys*. **26**, p. L1104 (1987).